Metrol. Meas. Syst., Vol. XXII (2015), No. 2, pp. 229–240.

PAN POLSKA AKADEMIA NAUK

METROLOGY AND MEASUREMENT SYSTEMS

Index 330930, ISSN 0860-8229

www.metrology.pg.gda.pl

M&MS

NOISE PROPERTIES OF THICK-FILM CONDUCTING LINES FOR INTEGRATED INDUCTORS

Adam Witold Stadler[1)], Andrzej Kolek[1)], Krzysztof Mleczko[1)], Zbigniew Zawiślak[1)], Andrzej Dziedzic[2)], Damian Nowak[2)]

1) Rzeszów University of Technology, Department of Electronics Fundamentals, Powstańców Warszawy 12, 35-959 Rzeszów, Poland (✉ astadler@prz.edu.pl, +48 17 865 1116, akoleknd@prz.edu.pl, kmleczko@prz.edu.pl, zawislak@prz.rzeszow.pl)

2) Wrocław University of Technology, Faculty of Microsystem Electronics and Photonics, Wybrzeże Wyspiańskiego 27, 50-370 Wrocław, Poland (Andrzej.Dziedzic@pwr.edu.pl, Damian.Nowak@pwr.edu.pl)

Abstract

Studies of noise properties of thick-film conducting lines from Au or PdAg conductive pastes on LTCC or alumina substrates are reported. Experiments have been carried out at the room temperature on samples prepared in the form of meanders by traditional screen-printing or laser-shaping technique. Due to a low resistance of the devices under test (DUTs), low-frequency noise spectra have been measured for the dc-biased samples arranged in a bridge configuration, transformer-coupled to a low-noise amplifier. The detailed analysis of noise sources in the signal path and its transfer function, including the transformer, has been carried out, and a procedure for measurement setup self-calibration has been described. The $1/f$ noise component originating from resistance fluctuations has been found to be dominant in all DUTs. The analysis of experimental data leads to the conclusion that noise is produced in the bends of meanders rather than in their straight segments. It occurs that noise of Au-based laser-shaped lines is significantly smaller than screen-printed ones. PdAg lines have been found more resistive but simultaneously less noisy than Au-based lines.

Keywords: low-frequency noise, thick-film conducting layer, thick-film inductor.

1. Introduction

Modern electronic circuits and modules require cheap, precise and reliable passive components. To fulfil these requirements, thick-film technology is widely used for the fabrication of resistors, capacitors, interconnecting lines and inductors [1]. In some cases, additional treatment is necessary in order to obtain components of precisely defined parameters, for example, a laser beam is used both for resistor trimming [2, 3] and resistive film cutting for precise defining the micro-resistor geometry [4]. Following this idea, we test usefulness of a laser beam for shaping inductors from a rectangular conductive film, previously deposited on various substrates. Various high-conductive lines, used for thick film inductors, have been prepared in the form of meanders in two ways: by traditional screen-printing and laser-shaping of conductive films. Electrical properties of the specimens have been examined with respect to their resistivity and low-frequency noise. Although in many RF applications such kind of noise may be neglected, there are classes of resonant circuits in which the resistance noise causes fluctuations of their Q-factor and selectivity, what may significantly degrade performance characteristics of the overall circuit.

The noise characterization of passive electronic components is getting more and more popular as it is much more sensitive to internal imperfections of materials or components than any other electrical test [5–9]. This technique can be also the source of important knowledge concerning stability and reliability of electronic components [10–13] indicating possible

Article history: received on Dec. 19, 2014; accepted on Feb. 14, 2015; available online on May 29, 2015; DOI: 10.1515/mms-2015-0021.

directions in technology improvement and development. Therefore, noise measurements are now an important method for characterization of new fabrication methods not only in micro- but also in nanotechnology [14, 15]. The other important reasons for testing noise properties of modern electronic components are related to (*i*) the fact that their geometrical size continuously decreases, what enhances the magnitude of low-frequency noise which is known to be inversely proportional to the device volume, (*ii*) the common trend of decreasing power dissipation in electronic modules which leads to low-level bias voltages, what relatively enhances the noise signal and forces the user/designer to take it into account, (*iii*) the fact that knowledge about noise sources may help in developing electrical transport models [16] and contributes to fundamental sciences.

2. Preparation of samples

Samples have been prepared on either alumina or LTCC substrates using Au or PdAg conducting pastes. On each substrate two meanders have been created in the same technological process. A laser beam was used for forming meanders from two rectangular, previously fired, conducting films of 4x10 mm^2 or 4x5 mm^2 size, so that half of the initial film surface was removed by the laser beam. In this way, two kinds of meanders have been obtained with their straight segments of either 10 mm or 5 mm length and 50 μm nominal width (see Fig. 1).

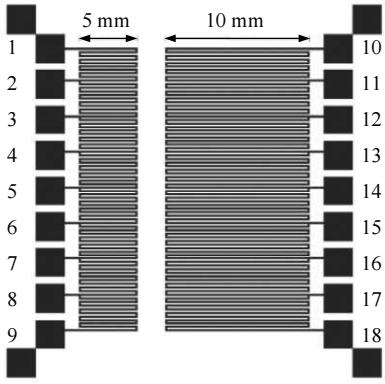

Fig. 1. The meander-like samples used in the experiments and contact enumeration.

The thickness of laser-shaped lines is equal to 7.5 μm. Another set of meander-like samples of the same shapes and dimensions has been prepared by the traditional screen-printing technique. In this case, the straight segments are 125 μm wide while their thickness is of 6 μm or 4.8 μm for films made of Au or PdAg pastes, respectively. In all meanders, the space between the segment lines is equal to their width.

3. Experiment

3.1. Measurement setup

Due to a low resistance of the samples, their low-frequency noise spectra have been measured using a transformer as the first amplification device in the signal path. The aim for using the transformer is to elevate the noise signal produced in samples above the noise floor of measurement circuitry. The measurement setup is shown in Fig. 2. The necessity for

rejection of dc bias (in order to protect the transformer) implies using a Wheatstone bridge with the sample under test, R_S, and a wire-wound variable resistor, $R = R_S$, in its bottom arms. Wire-wound resistors R_B of large resistance, $R_B >> R_S$, have been placed in the upper arms of the bridge. The bridge was dc-biased from a programmable voltage source via a low-pass filter with a large time constant. The transformer (type 233.7.1 from UNIPAN) has been used for coupling the signal from the bridge diagonal to a low-noise amplifier (type 5184 from Signal Recovery). After amplification, the signal was anti-alias (low-pass) filtered and connected to a DAQ-board, where the analogue-to-digital conversion took place. The digital signal processing, including calculation of its power spectral density, its averaging, spectra recording and presentation, was performed real-time using specialized software [17]. The spectra, averaged over 300 s, were recorded in the range $f < 5$ kHz with the resolution of 1 Hz.

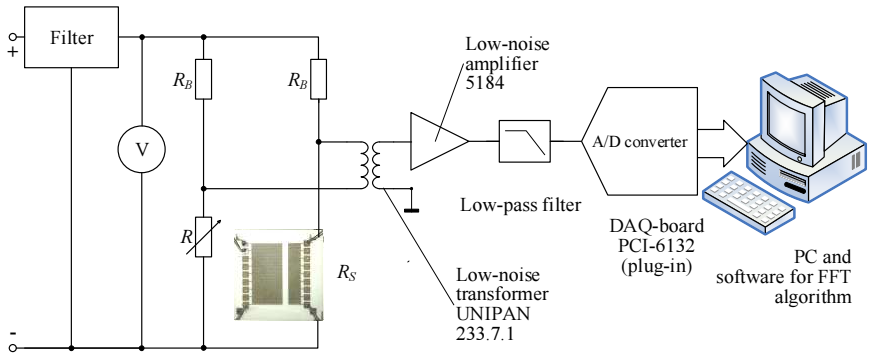

Fig. 2. The measurement setup for transformer-coupled low-level noise measurements.

3.2. Calibration of signal path

The transformer used in experiments has the secondary-to-primary turn ratio $N = 31.6$, and resistances $R_1 = 10\ \Omega$ and $R_2 = 15\ \text{k}\Omega$ of primary and secondary windings, respectively. Its transfer function G strongly depends on the sample resistance, and so the effective voltage ratio may differ from its nominal value N. Therefore, a special attention should be paid to calibration of the signal path. The noise model of measurement circuit shown in Fig. 3 includes the equivalent voltage and current noise sources, u_n and i_n , referred to the amplifier's input, the excess noise signal u_S, the noiseless input impedance Z_{in} of amplifier, and the linear transformer model. In the latter, the magnetic coupling of windings is described by current controlled voltage sources, M is the mutual inductance, L_1 and L_2 are self-inductances of the primary and secondary windings, $M = \sqrt{L_1 L_2} = NL_1$; $L_2 = N^2 L_1$, C_{TR} is the transformer output capacitance, and p is the coupling factor [18]. The thermal noise of bridge and transformer windings are represented by the sources e_{tS}, e_{t1}, e_{t2}.

The external resistance connected to the primary winding can be estimated as $R_S^{'} = 2R_S \,\|\, 2R_B \approx 2R_S$. On the other hand, the impedance seen at the transformer output, Z_{TRout}, which is significant for a further analysis, is given by (see Fig. 3):

$$Z_{TRout} = \left(\frac{\omega^2 p^2 M^2}{R_S + Z_1} + Z_2 \right) \| \frac{1}{j\omega C_{TR}}, \tag{1}$$

where $Z_1 = R_1 + j\omega L_1$, and $Z_2 = R_2 + j\omega L_2$. The plots of measured $|Z_{TRout}(\omega)|$ for different source resistances are shown in Fig. 4. $|Z_{TRout}|$ is suppressed for high frequencies by the capacitance C_{TR}. Its value, $C_{TR} \approx 0.24$ nF, has been extracted from the slope of line approximating $|Z_{TRout}(\omega)|$ in the range $f > 1$ kHz and for $R_S > 300\ \Omega$. The plot in the inset of Fig. 4 proves that values of $|Z_{TRout}|$ in the mid-frequency band are excellently fitted with the function $R_2 + N^2(R_1 + R_S)$. This means that in this frequency range the coupling factor is close to unity, $p = 1$ (strong magnetic coupling).

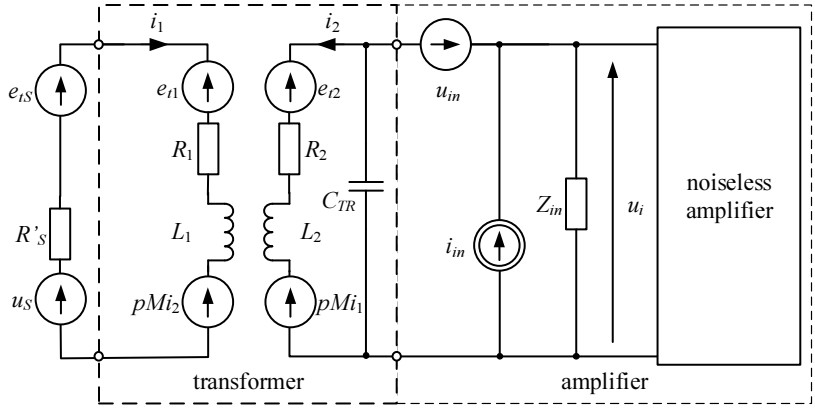

Fig. 3. The noise model of measurement circuit.

The frequency range where $|Z_{TRout}|$ is flat and constant strongly depends on the source resistance, and therefore using a transformer in noise measurement circuits is considered only for a low source resistance where the noise performance of transformer is optimal. Looking at the plots in Fig. 4, we may easily limit usefulness of the transformer approximately to $R_S < 300\ \Omega$. However, in the case of low-noise DUTs of higher resistance, transformer-coupling to the amplifier may be the only way for leveraging the device noise signal above the amplifier noise. This is the case of inductors made of conductive layers being under investigation in this paper.

The voltage at the amplifier input for the model from Fig. 3 is:

$$u_i = \left[\frac{-\dfrac{j\omega pM}{(R_S + Z_1)}(u_S + e_{tS} - e_{t1}) + e_{t2}}{1 + j\omega C_{TR} Z'_{TRout}} + u_n \right] \frac{Z_{in}}{Z_{TRout} + Z_{in}} + i_n (Z_{in} \| Z_{TRout}), \qquad (2)$$

where $Z'_{TRout} = 1/(1/Z_{TRout} - j\omega C_{TR})$ is the transformer output impedance without C_{TR}. For calibration purposes, we may use the thermal noise of source resistance as the wideband test signal. Assuming $u_S = 0$ (non-biased bridge), and switching to the power spectral density (p.s.d.), we immediately obtain the transfer function $G(\omega)$,

$$|G(\omega)|^2 = \left| -\frac{j\omega pM}{(R_S + Z_1)} \frac{Z_{in}}{Z_{TRout} + Z_{in}} \right|^2 = \frac{1}{1 + j\omega C_{TR} Z'_{TRout}} = \frac{S_{ui} - \left(\frac{4kTR_2}{\left|1 + j\omega C_{TR} Z'_{TRout}\right|^2} + S_{un} \right) \left| \frac{Z_{in}}{Z_{TRout} + Z_{in}} \right|^2 - S_{in} \left| Z_{in} \right| \left| Z_{TRout} \right|^2}{4kTR_S + 4kTR_1}. \tag{3}$$

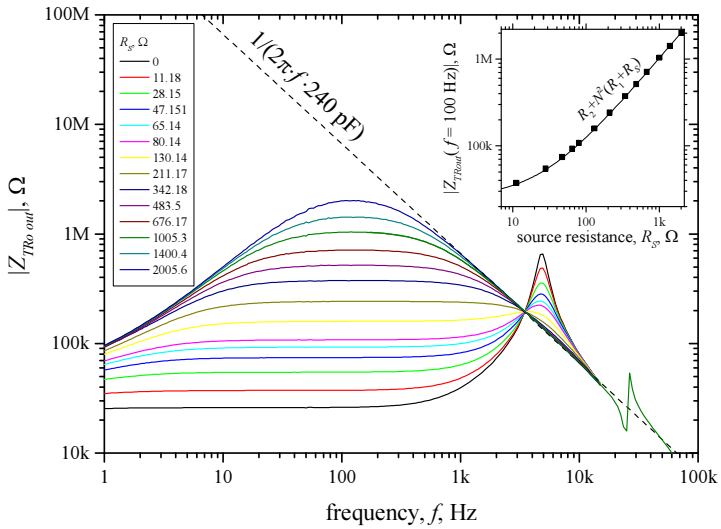

Fig. 4. The measured output impedance of transformer, $|Z_{TRout}|$, for different source resistances. The dashed line is the plot of impedance $1/|j\omega C_{TR}|$ for C_{TR} = 0.24 nF. Inset: $|Z_{TRout}(100\ \text{Hz})|$ vs. source resistance (points) and the function $R_2+N^2(R_1+R_S)$ (line).

The amplifier noise characteristics, S_{un}, and S_{in}, can be determined in standard short-circuited and open-input experiments. The results of such an experiment performed for the 5184 amplifier are shown in Fig. 5. The spectrum measured for the short-circuited amplifier refers to S_{un}. The other is for the open-input amplifier. The dashed line, fitting well with this spectrum for $f < 100$ Hz, refers to the thermal noise of amplifier input resistance R_{in}. This agreement proves that the equivalent input noise current of 5184 amplifier originates exclusively from the thermal noise of input resistance, *i.e.* $S_{in} = 4kT / R_{in}$. When the amplifier input is open, S_{in} produces the voltage noise:

$$S_{ui} = S_{in} \cdot |Z_{in}|^2 = \frac{4kT}{R_{in}} \cdot \left(\frac{R_{in}^2}{1 + \omega^2 \tau_{in}^2} \right) = \frac{4kTR_{in}}{1 + (\omega\tau_{in})^2}, \tag{4}$$

where $\tau = R_{in}C_{in}$ is the time constant of the parallel model of amplifier input impedance $Z_{in} = R_{in}||1/(j\omega C_{in})$. The dashed dotted line in Fig. 5, which exactly matches the measured p.s.d., is the plot of (4) with $\tau = 0.314$ ms. It gives the estimate of input capacitance, $C_{in} = 62.8$ pF, what is in excellent agreement with the description of 5184 [19].

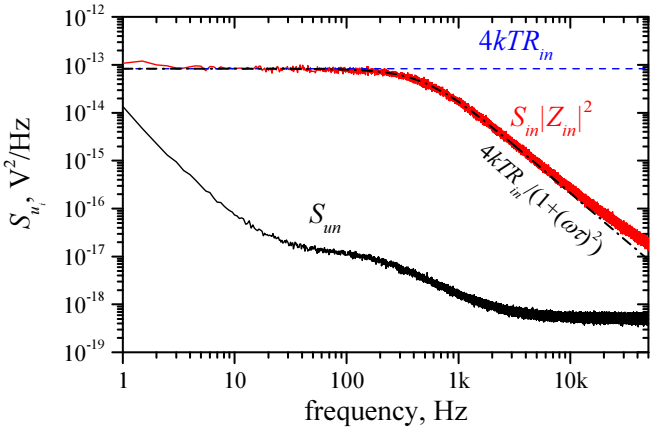

Fig. 5. The measured noise spectra of the 5184 amplifier for short-circuited (lower curve) and open input (upper curve). The dashed line is pinned at the value $4kTR_{in}$, where R_{in} = 5 MΩ. The dashed dotted line is the function graph of (4) for C_{in} = 62.8 pF.

Having the function $|G(\omega)|^2$ determined, we are ready to calculate the p.s.d. of excess noise, S_{uS}, in non-equilibrium measurements (biased bridge) when the signal u_S is nonzero. Making use of (3), we obtain:

$$S_{uS} = \frac{S_{ui} - \left(\dfrac{4kTR_2}{\left|1 + j\omega C_{TR} Z'_{TRout}\right|^2} + S_{un} \right) \left| \dfrac{Z_{in}}{Z_{TRout} + Z_{in}} \right|^2 - \dfrac{4kT}{R_{in}} \left| Z_{in} \parallel Z_{TRout} \right|^2}{|G|^2} - 4kT\left(R_S + R_1\right). \quad (5)$$

This formula was used in processing of the experimental data. The spectrum $S_{uS}(f)$ was identified with the DUT's excess noise, since it was the only source of excess noise in the measurement bridge (R_B and R are wire-wound excess-noise free resistors), and dumping the DUT's noise signal, u_{DUT}, by the load resistors R_B can be neglected, as:

$$u_S = u_{\mathrm{DUT}} R_B / \left(R_B + R_S\right) \approx u_{\mathrm{DUT}} . \quad (6)$$

To validate the above calibration procedure, additional experiments have been carried out. An unbiased wire-wound, low TCR, resistor (R_S = 676 Ω) has been connected to the transformer input and $G(\omega)$ has been calculated using (3) for the resistor kept either at the room or at 77.4 K (liquid nitrogen) temperature. This experiment provides the same value of source resistance, but a different magnitude of the test signal (thermal noise). The results are shown in Fig. 5 inset, together with the function $G(\omega)$ directly measured with a dynamic signal analyser (HP35660A). All three methods give almost the same function $G(\omega)$, which is correct, since G should depend on neither a method nor the magnitude of test signal. In Fig. 5, $|G|$ values averaged in the frequency band 40–100 Hz measured in above three ways are plotted as a function of the source resistance (points), giving again consistent results. As shown in Fig. 5, the values $\langle|G|\rangle$ agree also with the theoretical dependence derived for the circuit of Fig. 3. For the mid-frequency band ($|1 + j\omega C_{TR} Z'_{TRout}|^2 \approx 1$), one has:

$$G(\omega) = -j \frac{\omega p M}{R_S + Z_{TRin}} \frac{Z_{in}}{Z_{in} + Z_2} , \quad (7)$$

where Z_{TRin} is the input impedance of transformer loaded with the amplifier. In calculations of $\langle|G|\rangle$ with (7), the measured $Z_{TRin}(\omega)$ has been used.

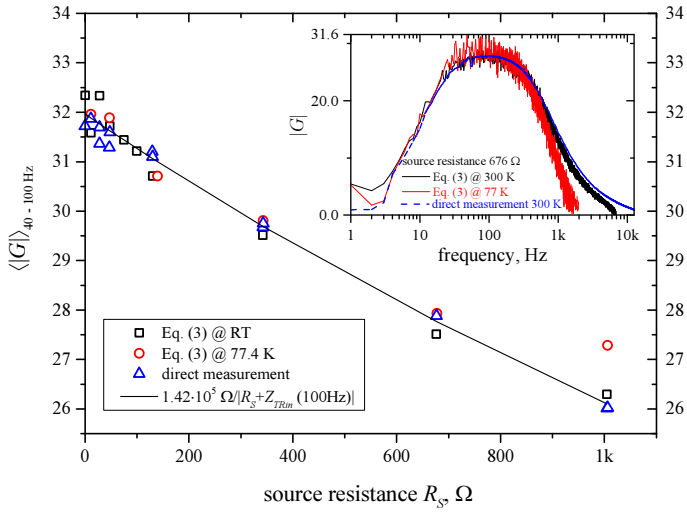

Fig. 6. The voltage ratio $|G|$ averaged over the frequency band 40–100 Hz obtained from the calibration procedure of (3), which uses the thermal noise of source resistor at either the room temperature (squares) or 77.4 K (circles), and the direct measurements using a dynamic signal analyser (triangles). The solid line is the plot of function 14.2 MΩ/|R_S+Z_{TRin}(100 Hz)| (see (7)). Inset: plots of $|G(\omega)|$ obtained in three different ways for R_S = 676 Ω.

4. Results

The exemplary collections of excess noise spectra gathered in Figs. 7a, 8a, 9a show that the 1/*f* noise is the dominant excess noise both for Au and PdAg samples, regardless of the fabrication process. The decreasing dashed line for the ideal 1/*f* noise has been plotted for reference. The horizontal solid line has been added to show the thermal noise $4kTR_S$ of sample resistance. Portions of the spectra that lie below the thermal noise are subjected to large variations due to the uncertainty of p.s.d. estimation resulting from subtraction of comparable values in (5).

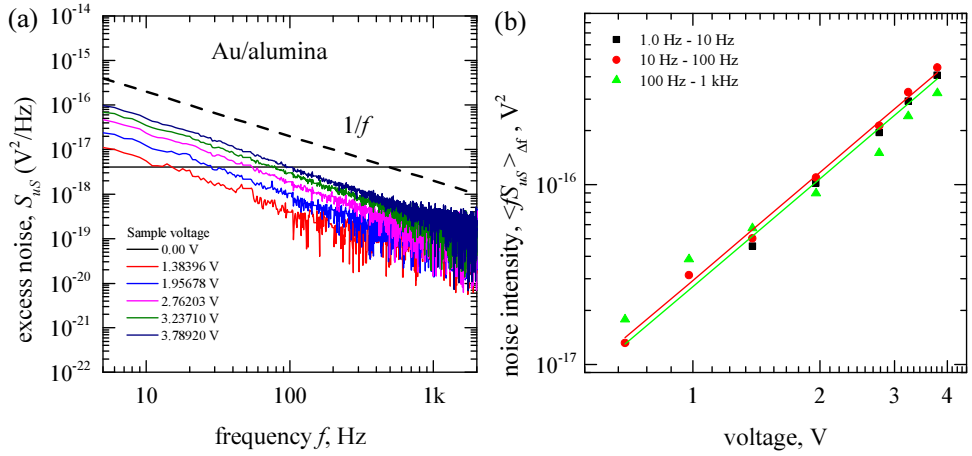

Fig. 7. a) The excess noise spectra, for different bias voltages, measured for laser-shaped Au on alumina substrate between terminals 1–9. The horizontal line shows the thermal noise of sample resistance; b) The noise intensity, calculated from data from Fig. 7a, in different frequency bands vs. bias voltage.

This can be improved when operands of this operation are less uncertain (*i.e.*, estimated with a large accuracy), what can be achieved by extending time of spectra averaging.

In the case of Fig. 8a, a relatively small sample voltage, $V < 1$ V, appeared to be sufficient to leverage the excess noise above the thermal noise in the studied frequency range. On the other hand, in Figs. 7a and 9a one can see that voltages V, $V > 1$ V, have to be applied in order to pull up the excess noise spectra above the thermal noise level.

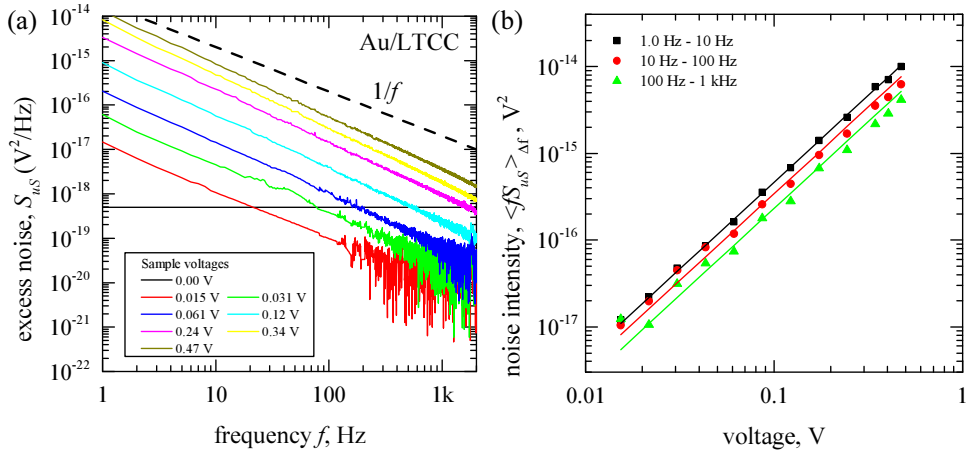

Fig. 8. a) The excess noise spectra vs, period bias voltage measured for screen-printed Au on LTCC substrate between terminals 1–9. The horizontal line shows the thermal noise of sample resistance; b) The noise intensity, calculated from data from Fig. 8a, in different frequency bands vs bias voltage.

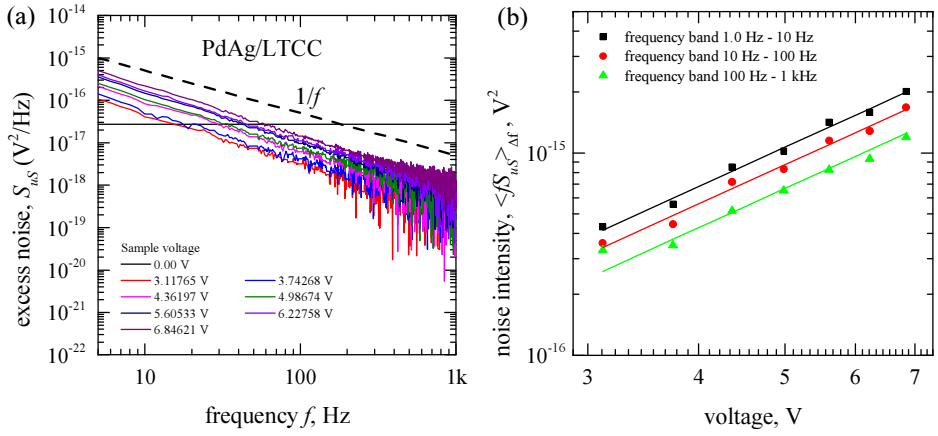

Fig. 9. a) The excess noise spectra for different sample voltages measured for screen-printed PdAg on LTCC substrate between terminals 10–18. The horizontal line shows the thermal noise of sample resistance;
b) The noise intensity, calculated from data taken from Fig. 9a, in different frequency bands vs. bias voltage.

5. Discussion

Since the $1/f$ noise is dominant in all studied samples, it is convenient to introduce the noise intensity defined as the product of frequency and power spectral density, $\langle fS_{uS}\rangle_{\Delta f}$, averaged over some frequency band Δf. This quantity is plotted in Figs. 7b, 8b, 9b, together with approximating lines versus bias voltage squared, V^2, evidencing that in all cases the noise

is caused by resistance fluctuations. The apparent discrepancy of noise intensity in different frequency bands is due to the spectral exponent different from 1 (usually $\gamma \geq 1$). The spectral exponent values, calculated from experimental data, have been gathered in Table 1. In all cases, the spectral exponent falls in the range $0.8 < \gamma < 1.2$, classifying the measured noise as $1/f$ phenomenon. The electro-migration noise, which gives a higher spectral exponent value of $\gamma \sim 2$ and is found in other conducting lines [20], must then be excluded.

Other columns of Table 1 include: the normalized noise intensity, $S = \langle fS_{uS} \rangle_{\Delta f} / V^2$, calculated for the frequency band $\Delta f = 10–100$ Hz, and the resistivity ρ. As can be seen, the resistivity and noise intensity data are widely scattered even for the same kind of samples. This is due to non-uniform line cross-sections which vary along the conducting path. These variations can be quite strong and even break the path making it discontinuous. In that case, measurements are only possible between intermediate probes (see case C, E, F). Nevertheless, paying enough caution when analysing the drawn data, some conclusions are still possible. Most important conclusion, which gives a view into the low-frequency noise generating mechanism, can be found for the case A. Samples 1–9 and 10–18 have the same number of bends, but the length of straight segments in sample 10–18 is twice of that of sample 1–9. The measured resistivity of both samples are the same, which ensures that they are connected with the bulk material. For the bulk origin of low-frequency noise, one expects the intensity, S, for sample 10–18 to be half of that of sample 1–9. However, the measured value of this ratio ~ $0.61/4.7 \approx 0.13$ is much lower. To some extent, an explanation of this discrepancy can be that, in fact, *the noise originates mainly from current crowding effects arising due to geometrical inhomogeneities* (width and thickness variations), which are mostly accumulated in the sharp bends of meanders. As the number of bends in both sample sets is the same, the noise voltage, S_V, for the same bias current should be also the same. For the normalized noise, this gives the S ratio equal to 1/4, as the bias voltage for sample 10–18 is twice of that for sample 1–9. In line with this explanation is the absolute value of estimated noise intensity. Taking into account sample dimensions, we estimate the material noise intensity, $C \equiv S \times$ *sample volume* $\sim 10^{-26}$ m^3 [21], which is 6 orders of magnitude larger than the value $C \sim 10^{-32}$ m^3 found for polycrystalline and single crystal Au films [22]. Although the structures of screen-printed and polycrystalline films are quite different, the resistivity of both samples in these two experiments were quite close (in [19] $\rho = 3–7$ Ωcm), so that an increase of the bulk noise due to different film structures cannot be that large and must have been enhanced by the current crowding effect.

Further conclusions are of practical importance:

- The noise intensity of Au-based conductors printed on LTCC substrates is always much larger than those printed on alumina. This is because rough LTCC surfaces enhance (add to) geometrical inhomogeneities of the stripes, what increases the noise.
- Laser shaping significantly decreases the noise and slightly increases the resistivity. This unusual behaviour (usually, the noise intensity increases linearly with resistivity) can be explained as resulting from the shaping process which smoothes line edges (decreases the electric field inhomogeneity and noise), simultaneously narrowing the effective width of the stripes (increases resistivity).
- The PdAg material gives more resistive but less noise conducting lines. However, using this material in low-noise applications/circuitry is not obvious, as PdAg line itself would produce a lower noise, but simultaneously introduce more noise coming from common mode signals.

Table 1. The electrical and noise properties of studied samples at the room temperature.

Technology	Conducting Layer	Substrate /Case	Terminals	Parameter		
				ρ, Ω cm	S	Spectral exponent
Screen-printing	Au	alumina A	(1–9)	$2.4 \cdot 10^{-6}$	$4.7 \cdot 10^{-15}$	1.15
			(10–18)	$2.5 \cdot 10^{-6}$	$6.1 \cdot 10^{-16}$	1.20
		LTCC B	(1–9)	$2.8 \cdot 10^{-6}$	$3.5 \cdot 10^{-14}$	1.18
			(10–18)	$4.0 \cdot 10^{-6}$	$2.4 \cdot 10^{-15}$	1.12
	PdAg	alumina C	(1–9)	$3.8 \cdot 10^{-5}$	$8.0 \cdot 10^{-16}$	1.05
			(10–17)	$5.1 \cdot 10^{-5}$	$9.1 \cdot 10^{-17}$	0.89
		LTCC D	(1–9)	$3.26 \cdot 10^{-5}$	$9.6 \cdot 10^{-16}$	1.08
			(10–18)	$6.19 \cdot 10^{-5}$	$3.5 \cdot 10^{-17}$	1.14
Laser-shaping	Au	alumina E	(1–9)	$5.77 \cdot 10^{-6}$	$2.9 \cdot 10^{-7}$	1.16
			(14–18)	$5.6 \cdot 10^{-6}$	$3.8 \cdot 10^{-17}$	1.12
	Au	LTCC F	(2–9)	$5.7 \cdot 10^{-6}$	$1.4 \cdot 10^{-16}$	1.16

6. Summary

The low-frequency noise of conductive paths made of materials widely used in thick-film technology, *i.e.*, Au and PdAg pastes, has been measured and analysed. The sample meanders have been made on alumina or LTCC substrates by traditional screen-printing or by laser-shaping. Due to a low resistance and noise of the samples, the measurement setup with a dc Wheatstone bridge and a coupling transformer had to be employed and was thoroughly analysed in the paper. In all studied samples, the $1/f$ noise caused by resistance fluctuations has been found. It occurs that this noise is generated in sharp bends of the conducting path, rather than in the bulk of the conductors. An important observation is that the noise intensity in laser-shaped inductors is significantly smaller than in screen-printed stripes. Furthermore, the analysis of resistivity of studied inductors indicates that a laser beam modifies electrical properties of the edge of conducting path. Moreover, the noise of inductors made of Au is substrate-sensitive.

These results may be used in design and optimization of the manufacturing process of thick-film inductors. Sharp bends should be avoided, and circular rather than rectangular-shaped inductors should be designed. At the moment, laser-shaped Au-based devices seem to offer better Q-factor and noise performance. To the Authors' knowledge, this is the first analysis of the low-frequency noise of conducting thick-film lines that can be used for integrated inductors.

Acknowledgements

The work has been supported from Grant DEC-2011/01/B/ST7/06564 funded by National Science Centre (Poland) and from Rzeszow University of Technology, Department of Electronics Fundamentals Grant for Statutory Activity (DS). Studies have been performed with the use of the equipment purchased in the project No. POPW.01.03.00-18-012/09 from

the Structural Funds, The Development of Eastern Poland Operational Programme co-financed by the European Union, the European Regional Development Fund.

References

[1] Bhattacharya, S.K., Tummala, R.R. (2000). Next generation integral passives: materials, processes, and integration of resistors and capacitors on PWB substrates. *Journal of Material Science: Materials in Electronics*, 11, 253–268.

[2] Chun-Hao, L., Ming-Jong, T. (2009). 3D laser trimming technology for regulating embedded thick-film carbon resistors on a random access memory module. *Journal of Materials Processing Technology*, 209, 2057–2067.

[3] Dziedzic, A., Kolek, A., Ehrhardt, W., Thust, H. (2006). Advanced electrical and stability characterization of untrimmed and variously trimmed thick-film and LTCC resistors. *Microelectronics Reliability*, 46, 352–359.

[4] Stadler, A.W., Zawiślak, Z., Dziedzic, A., Nowak, D. (2014). Noise spectroscopy of resistive components at elevated temperature. *Metrol. Meas. Syst.*, 21, 15–26.

[5] Rocak, D., Belavic, D., Hrovat, M., Sikula, J., Koktavy, B., Pavelka, J., Sedlakova, V. (2001). Low-frequency noise of thick-film resistors as quality and reliability indicator. *Microelectronics Reliability*, 41, 531–542.

[6] Jevtić, M.M., Mrak, I., Stanimirović, Z. (1999). Thick-film quality indictor based on noise index measurements. *Microelectronics Journal*, 30, 1255–1259.

[7] Jevtić, M.M. (1995). Noise as a diagnostic and prediction tool in reliability physics. *Microelectronics Reliability*, 35, 455–477.

[8] Zarnik, M.S., Belavic, D., Sedlakova, V., Sikula, J., Kopecky, M., Sedlak, P., Majzner, J. (2013). Comparison of the intrinsic characteristics of LTCC and silicon pressure sensors by means of 1/*f* noise measurements. *Radioengineering*, 22(1), 227–232.

[9] Bobalo, Y., Kolodiy, Z., Stadnyk, B., Yatsyshyn, S. (2013). Development of noise measurements. part 3. Passive method of electronic elements quality characterization. Sensors *and Transducers*, 152, 164–168.

[10] Dziedzic, A. (2002). Electrical and structural investigations in reliability characterisation of modern passives and passive integrated components. *Microelectronics Reliability*, 42, 709–719.

[11] Kolek, A. (2006). *Experimental methods of low-frequency noise*. University of Technology Publications, Rzeszow, Poland.

[12] Stadler, A. (2011). Noise properties of thick-film resistors in extended temperature range. *Microelectronics Reliability*, 51, 1264–1270.

[13] Mleczko, K., Zawiślak, Z., Stadler, A.W., Kolek, A., Dziedzic, A., Cichosz, J. (2008). Evaluation of conductive-to-resistive layers interaction in thick-film resistors. *Microelectronics Reliability*, 48, 881–885.

[14] Balandin, A.A. (2013). Low-frequency 1/*f* noise in graphene devices. *Nature Nanotechnology*, 8(8), 549–555.

[15] Granqvist, C.G., Green, S., Jonson, E.K., Marsal, R., Niklasson, G.A., Roos, A., Topalian, Z., Azens, A., Georén, P., Gustavsson, G., Karmhag, R., Smulko, J., Kish, L.B. (2008). Electrochromic foil-based devices: Optical transmittance and modulation range, effect of ultraviolet irradiation, and quality assessment by 1/*f* current noise. *Thin Solid Films*, 516(17), 5921–5926.

[16] Stadler, A.W., Kolek, A. (2007). Numerical simulations of low-frequency noise in RuO_2-glass films. *Proc. SPIE* 6600, 66000Q.

[17] Stadler, A. (2011). Virtual instruments in low-frequency noise spectroscopy experiments. *Proc. 35th Int. Conf. of IMAPS-CPMT Poland Chapter*, Gdańsk-Sobieszewo, 311–316.

[18] Lepaisant, J., Lam Chok Sing, M., Bloyet, D. (1992). Low-noise preamplifier with input and feedback transformers for low source resistance sensors. *Rev. Sci. Instrum.*, 63, 2089–2094.

[19] Model 5184 Ultra Low Noise Preamplifier. *www.signalrecovery.com*

[20] Neri, B., Ciofi, C., Dattilo, V. (1997). Noise and fluctuations in submicrometric Al-Si interconnect lines. *IEEE Transactions On Electron Devices*, 44(9), 1454–1459.

[21] Dziedzic, A., Kolek, A. (1998). 1/*f* noise in polymer thick-film resistors. *Journal of Physics D: Applied Physics*, 31, 2091–2097.

[22] Verbruggen, A.H., Koch, R.H., Umbach, C.P. (1987). Correlation between 1/*f* noise and grain boundaries in thin gold films. *Phys. Rev. B.*, 35, 5864–5867.